JOURNAL OF COMPUTATIONAL PHYSICS 98, 301–316 (1992)

# Hydrodynamic Modeling of Particle and Angular Momentum Transport in Rotating Tokamak Plasmas with Impurities

R. ZANINO

*Energetics Department, Polytechnic Institute of Turin, Italy*

Received April 25, 1990

We have developed a 1 + 1 D time dependent code for the description of ion-impurity transport in a rotating tokamak plasma, using a pseudo-spectral discretization in the poloidal angle $\theta$ and a staggered finite difference mesh in the minor radius $r$. The plasma is assumed to have a constant uniform temperature $T$, to be in the high collisionality (Pfirsch–Schlüter) regime, and to contain electrons "$e$," fuel ions "$i$," and a single impurity species "$Z$" of charge $eZ$, where $e$ is the proton charge. We are particularly interested in the case when: (1) flow velocities in the toroidal (symmetry) direction $\phi$ are in the range typical of neutral beam injection experiments, i.e., $v_{thZ} < V_{\phi i,Z} \lesssim v_{thi}$, ($v_{thj} \equiv \sqrt{2T/m_j}$ is the thermal speed, $m_j$ is the mass); (2) the relative concentration of impurities in the plasma, $\bar{n}_Z/\bar{n}_i$, is significant and comparable to that observed in present tokamaks, i.e., $\sqrt{m_e/m_i} \ll \bar{n}_Z Z^2/\bar{n}_i \approx 1$ in order of magnitude. The model fluid equations are obtained via a moment approach, and an expansion in powers of the small ordering parameter $\delta_{pi} \equiv (m_i v_{thi}/eB_\theta)$ $((1/\bar{n}_i)\,|\partial \bar{n}_i/\partial r|) \ll 1$ ($\mathbf{B}$ is the magnetic field) is then employed. The equations at each order in $\delta_{pi}$ up to the second are solved, and the characteristic features of the results presented: to lowest order, outboard impurity peaking on each magnetic surface appears due to centrifugal forces; to first order, radial gradients driven ion-impurity friction gives rise to up–down asymmetries in the poloidal profiles; to second order, the radial profiles of density and rotation frequency evolve to steady state under the action of particle and angular momentum sources. The evolution of the poloidal profiles is decoupled from the evolution of the radial ones, thanks to the fact that the corresponding time scales belong to different orders in $\delta_{pi}$: an algorithm is proposed to treat the 2D problem, alternating the solution of 1D problems. 

## 1. INTRODUCTION

Control of the impurities concentration in the plasma constitutes a critical issue in present and future fusion experiments. As a measure of the collisional effects due to the presence of impurities in the plasma one can introduce the parameter

$$Z_{\text{eff}} \equiv \sum_k \frac{n_k Z_k^2}{n_e}, \tag{1}$$

where the sum runs over all ion species (fuel and impurities), $n_k$ is the density of the $k$th ion species of charge $eZ_k$, and $n_e$ is the electron density. While in a pure plasma $Z_{\text{eff}} = 1$, typically observed values are $\gtrsim 2$; if one assumes for simplicity that a single impurity species "$Z$" is present in the plasma, it is therefore interesting to consider the case when its concentration is such that

$$\alpha \equiv \frac{n_Z Z^2}{n_i} \approx 1 \tag{2}$$

in order of magnitude, because if $Z \gg 1$ then $Z_{\text{eff}} \approx 1 + \alpha$. If (2) is satisfied, ion-impurity collisions are the main collisional mechanism for ion transport since, when all species have the same temperature,

$$\frac{v_{ie}}{v_{iZ}} \sim \frac{(m_e n_e/m_i n_i)\, v_{ei}}{(n_Z Z^2/n_i)\, v_{ii}} \sim \sqrt{m_e/m_i} \ll 1 \tag{3}$$

(here $v_{jk}$ is the inverse of the characteristic time required for a particle of species $j$ to be scattered by 90° by collisions with particles of species $k$ [3], and $m_j$ is the mass of the particle), i.e., the effect of ion–electron collisions on the ions is negligible.

When for a given species the total collision frequency is much larger than the transit frequency (see (9)), a fluid description of that species is justified. The issue of impurity transport in toroidal magnetic configurations, in the limit of high (Pfirsch–Schlüter) collisionality, was first addressed in [4]. The resulting so-called neoclassical theory of impurity transport—the word "neoclassical" is generally used here to denote features due to the toroidal geometry, as compared to the classical effects already present in a cylindrical plasma—can be very relevant to experiments because the particle diffusion coefficient $D$ scales as

$$D_{\text{impure}} \sim \rho_{\theta i}^2 \nu_{iZ} \gg D_{\text{pure}} \sim \rho_{\theta e}^2 \nu_{ei}, \tag{4}$$



0021-9991/92 $3.00

where $\rho_{\theta j} \equiv m_j v_{thj}/eZ_j B_\theta$ is the Larmor radius in the poloidal magnetic field, and $v_{thj} \equiv \sqrt{2T/m_j}$ is the thermal speed. From (3) and (4) we see that, in the case of an impure plasma as compared to a pure one, the theory is nearer by a factor of $\sqrt{m_i/m_e}$ to explain the relatively small particle confinement times observed in present tokamaks.

The practical interest for the effects of finite impurity flow velocities compared with the ion thermal speed (see, e.g., [5] for an early reference to this point) arises in the context of neutral beam heated tokamak plasmas. When the neutral injection is toroidally unbalanced it also provides an *axial* angular momentum source for the plasma, and measured [6] toroidal flow velocities are in the range

$$v_{thZ} < V_{\phi i,Z} \lesssim v_{thi}. \tag{5}$$

Ion-impurity transport in a strongly rotating tokamak plasma is intrinsically two-dimensional. Differently from the case of small rotation, where the densities and the electric potential are in first approximation flux surface functions, inertial forces induce significant variations of those parameters on a given magnetic surface, as soon as the flow velocities become comparable to the thermal speed. (We notice, however, that also in slowly rotating plasmas, sensible poloidal variations of the pressure of the single species can arise, provided the ion-impurity friction is sufficiently large [7].)

Neoclassical transport in strongly rotating impure tokamak plasmas has been studied in a number of papers ([8–10], and references therein). In particular, a fluid theory was proposed in [9], where a non-classical drag mechanism was able to explain the rate of radial transfer of axial angular momentum measured in the experiments, which is exceedingly large when compared with neoclassical theory predictions to date. Both in [8, 9] it was assumed sufficient to approximate variations in poloidal angle through a Fourier expansion truncated to the first harmonic, and the amplitude of this modulation compared to the average value was taken as small in the plasma inverse aspect ratio $\varepsilon \equiv a/R_0$ ($a$ and $R_0$ are the minor and major plasma radius, respectively). This allows an analytic treatment, but quickly becomes inadequate, when the rotation is very large, and causes variations on the surface comparable to the average value [13].

From a physical point of view the model discussed in the present paper contains, as compared to previous ones, all and only the purely classical and neoclassical contributions (no ad hoc terms) in the short mean free path regime; in particular, inertial viscous and friction effects pertaining to a strongly rotating tokamak plasma are included.

From a computational point of view, one must solve a system of time-dependent, nonlinear partial differential equations (PDE) in two space dimensions (axisymmetry is assumed in the third, toroidal coordinate). We propose here an algorithm that allows us to solve this 2D evolution problem, alternating the integration of 1D systems in each of the two space directions. The method is tailored to the physics of the problem and takes full advantage of the fact that the profiles in radius and poloidal angle evolve neoclassically on separate time scales. Furthermore, we can afford, in principle, arbitrarily large poloidal variations of the relevant plasma parameters.

The model we present and solve here was derived in detail in [1], and preliminary results were already presented in [23]. The major features of the model are reviewed in Section 2. Ordering in one small parameter is used to obtain equations which describe the system on three different time scales; in Section 3 the lowest order (fastest) scale is considered; in Section 4 the intermediate one and in Section 5 the slowest one. Conclusions are summarized in Section 6.

## 2. GENERAL FEATURES OF THE MODEL

We give here an overview of the hydrodynamic model of ion-impurity transport in a strongly rotating collisional tokamak plasma, which is discussed in the next sections. By taking velocity moments of the Fokker–Planck equation one can build a hierarchy of fluid equations. This hierarchy can be truncated, assuming the plasma is in the high collisionality Pfirsch–Schlüter regime; in that case, in fact, the dependence of the distribution function $f_j$ of the generic particle species $j$ on the pitch angle is sufficiently smooth to be approximated by an expansion containing Legendre polynomials up to only quadratic terms.

The unknowns of the system are now the moments of $f_j$, and they can be expanded in powers of a small parameter. In tokamaks the magnetic field is strong enough to render the ratio between the ion Larmor radius and the typical radial scale length very small. Furthermore, the confinement in tokamaks is provided by the poloidal component of the field, so that it is customary [11] to use the ratio

$$\delta_{pi} \equiv \frac{\text{ion Larmor radius in the poloidal field}}{\text{characteristic radial scale length}} \ll 1 \tag{6}$$

as the small expansion parameter. In order to be able to describe radial transport with the model it will be sufficient to retain terms up to the second order in this expansion [5, 11]. Notice also that the ordering in $\delta_{pi}$ breaks down in the region of divertor tokamaks near the $X$-point, where the poloidal field goes to zero: our model, therefore, will not be applicable in that region.

In the time independent problem the essential point in

using the expansion in $\delta_{pi}$ is that each of the moment equations contains terms arising from the term $e_j n_j \mathbf{v}_j \times \mathbf{B} \cdot \nabla_v f_j$ in the kinetic equation; those terms have the form $\mathbf{A} \times \mathbf{B}$, where $\mathbf{A}$ is a generic tensor flux. Since $\mathbf{B}$ is the large marking parameter, the equation to $O(\delta_{pi}^{k-1})$ will determine the flux $\mathbf{A}_\perp^{(k)}$, which is perpendicular to $\mathbf{B}$, as a function of lower order quantities. The parallel fluxes $\mathbf{A}_\parallel^{(k)}$ then have to be solved for as functions of $\mathbf{A}_\perp^{(k)}$ [1].

In the time-dependent problem one can use a multiple time scale expansion of the form

$$\frac{\partial}{\partial t} = \frac{\partial}{\partial t_0} + \frac{\partial}{\partial t_1} + \frac{\partial}{\partial t_2} + \cdots \tag{7}$$

whereby, defining

$$\tau_k \approx \left( \frac{\partial}{\partial t_k} \log y \right)^{-1} \tag{7'}$$

and $y$ being any variable representative of the state of the plasma, one simply means that $\tau_k / \tau_{k+1} \approx O(\delta_{pi})$.

It is easy to get a qualitative idea of the relationship between the fastest ($\tau_0$) and the slowest ($\tau_2$) time scales considered in this paper. Let us start by comparing the time derivative term with, e.g., the pressure gradient, in the ion parallel momentum balance to lowest order; one obtains

$$B m_i n_i \frac{\partial V_{\parallel i}}{\partial t_0} \sim -T \mathbf{B} \cdot \nabla n_i \tag{8}$$

and for $V_{\parallel i} \approx v_{thi}$

$$\tau_0 \approx \left( \frac{(B_\theta / B)\, v_{thi}}{a} \right)^{-1} \equiv \omega_{ti}^{-1}, \tag{9}$$

where we have introduced the ion transit frequency $\omega_{ti}$. Notice that the fastest evolution ends when one reaches equilibrium *separately* on each flux surface, i.e., $\tau_0$ is the time scale for the evolution of the poloidal profiles. We will see in Section 3 that the equations for the zeroth order steady state contain only poloidal derivatives.

In order to estimate the slowest time scale consider a simple radial diffusion equation

$$\frac{\partial \bar{n}_i}{\partial t_2} = \frac{1}{r} \frac{\partial}{\partial r} \left( r D \frac{\partial \bar{n}_i}{\partial r} \right) \tag{10}$$

(we will obtain in Section 5.1 analogous equations by flux surface averaging general balances, thereby annihilating the poloidal derivatives). From neoclassical theory [4] the diffusion coefficient scaling is $D \approx \rho_{\theta i}^2 \nu_{iZ}$, and one obtains from (10)

$$\tau_2 \approx \left( \delta_{pi}^2 \frac{\nu_{iZ}}{\omega_{ti}} \omega_{ti} \right)^{-1} \approx \frac{\tau_0}{\delta_{pi}^2}. \tag{11}$$

Comparing (9) and (11) it follows that the evolution of the *radial* profiles is very much slower (by two orders in $\delta_{pi}$) than the evolution of the *poloidal* ones. This points to the possibility of decoupling the full 2D evolutionary problem into the alternating solution of 1D problems: such a strategy will be developed in the next sections.

A few symplifying assumptions are used in the present paper. First, a uniform and constant temperature $T$, the same for all species, is assumed, obtaining in this way a dramatic reduction in the complexity of the model. (Recently, however, a theory has been presented including the plasma energy balance [21]). The rationale here is that we are mainly interested in studying the confinement of particles and particularly angular momentum from the point of view of collisional neoclassical theory, where the key role is played by the interspecies friction forces: since the thermal force [3] is known to give a comparable (not dominant) contribution to friction as the difference in flow velocities, we do not expect our results to be qualitatively wrong due to this simplification. Following (2) and (3) it is then further assumed that a single impurity species is present in the plasma, with a sufficiently large concentration to make negligible for ion species the effect of collisions with the electrons. Finally, a low beta large aspect ratio equilibrium with fixed circular concentric magnetic surfaces constitutes the background for the numerical solution of the transport model.

## 3. ZEROTH-ORDER TIME SCALE

The purpose of this section is to compute the flow field and the poloidal distribution of the various particle densities, in the steady state reached when the zeroth-order time scale transient is extinguished. We already obtained elsewhere [13] the zeroth-order steady state also as a result of time evolution; here the equations are solved directly for steady state considering that they describe the fastest time scale in our model.

An analysis of the moment equations [1, 12], shows that to zeroth order in $\delta_{pi}$ the flow on each magnetic surface is purely rigid toroidal and species independent, i.e.,

$$\mathbf{V}_j^{(0)} = \omega^{(0)}(r)\, R \hat{\mathbf{e}}_\phi. \tag{12}$$

To determine the density variation on the surface one uses

then the parallel momentum balance to zeroth order for ions and impurities

$$-\frac{1}{2}m_j\omega^{(0)2}\frac{\partial}{\partial\theta}R^2 = -T\frac{\partial}{\partial\theta}\log n_j^{(0)} - eZ_j\frac{\partial}{\partial\theta}\Phi^{(0)} \tag{13}$$

and the corresponding balance for the electrons, where inertia can be neglected,

$$0 = -T\frac{\partial}{\partial\theta}\log n_e^{(0)} + e\frac{\partial}{\partial\theta}\Phi^{(0)}. \tag{14}$$

The electrostatic potential $\Phi^{(0)}$ can then be eliminated, imposing quasineutrality of the plasma,

$$n_e^{(0)} = n_i^{(0)} + Zn_Z^{(0)}. \tag{15}$$

The set (13)–(15) can be solved straightforwardly [10]. The solution is

$$n_j^{(0)}(r,\theta) = \bar{n}_j(r)\frac{A_j^{(0)}}{\langle A_j^{(0)}\rangle}, \tag{16}$$

where we have introduced the flux surface averaged density $\bar{n}_j$ and we have defined

$$A_j^{(0)}(r,\theta) \equiv \exp\left(\frac{m_j\omega^{(0)2}R^2}{2T}\right) \times\left[\frac{n_i^{(0)}(\theta=0)+Zn_Z^{(0)}(\theta=0)}{n_i^{(0)}+Zn_Z^{(0)}}\right]^{Z_j}, \tag{17}$$

and the flux surface average of an arbitrary function $y$ of the poloidal angle,

$$\langle y(\theta)\rangle \equiv \frac{\int_0^{2\pi} y(\theta)\,R(\theta)\,d\theta}{2\pi R_0}, \tag{18}$$

for circular concentric magnetic surfaces with $R(\theta)\equiv R_0 - r\cos\theta$; notice the coordinate system is chosen such that $\theta=\pi$ outboards.

The solution (16), (17) is in strongly implicit form; therefore a simple iteration [2] is used to obtain the explicit solution. At this level the flux surface functions $\bar{n}_j$ and $\omega^{(0)}$ are considered as given, since their radial profiles evolve much more slowly.

As an example of a typical result of the zeroth order computation, poloidal profiles of the ion (dashed line) and impurity (solid line) densities are shown in Fig. 1, normalized to their respective flux surface average. The profiles refer to the surface which lies at $r=a/2$, and for the quantities evolving only on the second-order time scale we chose the values MACH = 0.75, where the ion Mach number is defined as

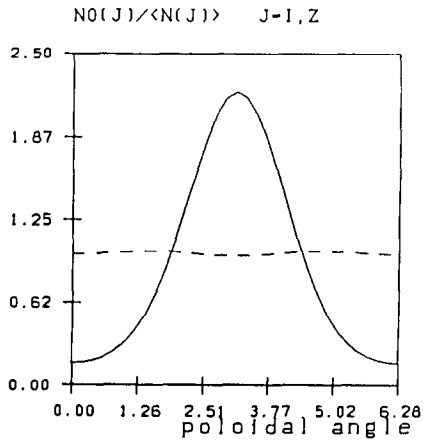


FIG. 1. Zeroth-order steady state solution, as a function of poloidal angle $\theta$: $n_i^{(0)}/\bar{n}_i$ (dashed line), $n_Z^{(0)}/\bar{n}_Z$ (solid line). Notice $\theta=\pi$ outboards.

$$\mathrm{MACH}(r) \equiv \frac{\omega^{(0)}(r)\,R_0}{v_{thi}}, \tag{19}$$

ion average density $\bar{n}_i = 6.0\times10^{19}m^{-3}$, and impurity average density $\bar{n}_Z$ such that $\bar{\alpha}\equiv\bar{n}_Z Z^2/\bar{n}_i = 1$; the impurity species is oxygen with $Z=6(O^{6+})$, as for all the other numerical examples presented in this paper unless otherwise noted. One observes in Fig. 1 the strong nonlinear outboard peaking of the impurity density due to the centrifugal force, whereas the ions, being still subsonic contrary to the impurities, mainly feel the effect of the parallel electric field, resulting in an outboard hollow profile.

When the computation is repeated on surfaces located at different minor radii, the 2D distribution of the impurity density on the plasma cross section results as shown in Fig. 2. The amplitude of the modulation in the poloidal density profiles and, in particular, the outboard hollowness of the ions, depend on the value of the ratio

$$\zeta \equiv \frac{m_Z}{Zm_i}. \tag{20}$$

To illustrate this point, the zeroth order steady state densities for the same case of Fig. 1 but taking now $O^{2+}$ as the impurity species are given in Fig. 3. The dependence on $\zeta$ can be qualitatively explained [2] in the limit $\bar{\alpha}\ll 1$ by linearising (16)–(17).

We finally remark that the most important feature of the zeroth order results is that the densities are up–down symmetric; this comes from the fact that ion-impurity friction vanishes because of (12), and consequently there is no neoclassical radial transport to this order.

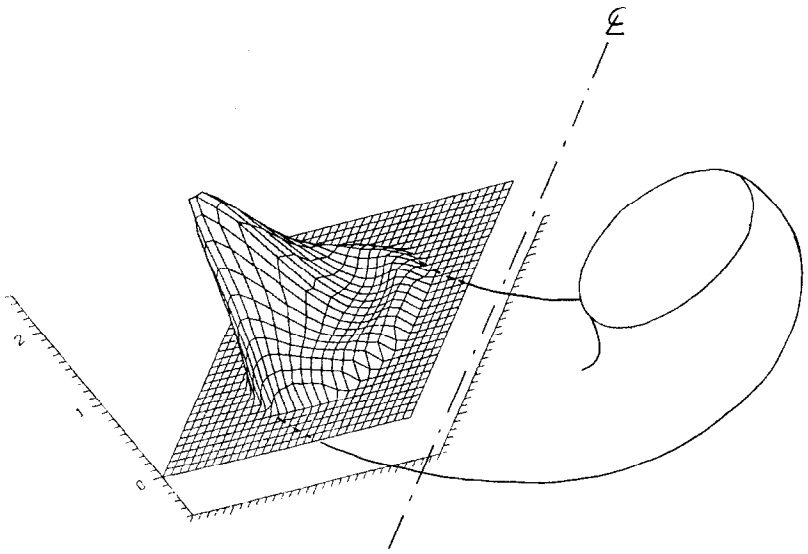

FIG. 2. Two-dimensional impurity density distribution $n_Z^{(0)}(r, \theta)/\bar{n}_Z$ ($r = 0$) over the plasma cross section; parabolic radial profiles are assumed.

## 4. EVOLUTION ON THE FIRST-ORDER TIME SCALE

### 4.1. *Equations*

As in the case of negligible rotation it can be shown [1] that the flow up to first order lies on the magnetic surfaces and therefore can be decomposed in parallel and diamagnetic components

$$\mathbf{V}_j \equiv V_{\|j}\hat{\mathbf{b}} + \frac{B_\theta}{B}\omega_j R\hat{\mathbf{e}}_\perp, \tag{21}$$

where

$$\omega_j(r, \theta) \equiv \omega^{(0)}(r) + \omega_j^{(1)}(r, \theta). \tag{21'}$$

Using the zeroth order solution, the zeroth order momentum balance in the direction perpendicular to the magnetic surfaces gives, for each of the two-ion species ($j = i, Z$), the first-order diamagnetic flow,

$$\omega_j^{(1)} \equiv \frac{B}{\Omega_j}\left(\frac{R}{B_\theta}\omega^{(0)}\frac{\partial\omega^{(0)}}{\partial r} + \frac{T}{m_j}\frac{1}{RB_\theta}\frac{\partial}{\partial r}\log\frac{\bar{n}_j}{\langle A_j^{(0)}\rangle}\right), \tag{22}$$

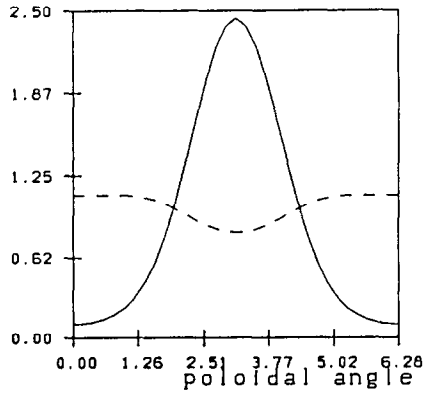


FIG. 3. Same as Fig. 1, except $O^{2+}$ is the impurity instead of $O^{6+}$.

where $\Omega_j \equiv eZ_jB/m_j$ is the Larmor frequency. It is important to notice in (22) that the first term on the right-hand side is a completely new contribution to the diamagnetic flow coming from the strong rotation of the plasma, while the second term reduces for negligible rotation to the well-known $\mathbf{E}\times\mathbf{B}$ and $\nabla p\times\mathbf{B}$ drifts [11].

The equations which approximately describe the evolution on the first-order time scale are the continuity equation

$$\frac{\partial n_j}{\partial t} = -\frac{B_\theta}{B}\frac{1}{Rr}\frac{\partial}{\partial\theta}\left[Rn_j\left(V_{\|j} + \frac{B_\phi}{B}\omega_j R\right)\right] \tag{23}$$

and the parallel momentum balance

$$\begin{aligned}\frac{\partial V_{\|j}}{\partial t} = &-\left(V_{\|j} + \frac{B_\phi}{B}\omega_j R\right)\hat{\mathbf{b}}\cdot\nabla\left(V_{\|j} + \frac{B_\phi}{B}\omega_j R\right)\\ &+\left(V_{\|j} + \frac{B_\phi}{B}\omega_j R\right)\frac{B_\phi}{B}R\hat{\mathbf{b}}\cdot\nabla\omega_j\\ &+\frac{\omega_j^2}{2}\hat{\mathbf{b}}\cdot\nabla R^2 - \frac{B_\theta}{B}\frac{T}{m_j}\frac{\partial}{r\partial\theta}\log n_j\\ &-\frac{B_\theta}{B}\frac{Z_j}{m_j}T\frac{\partial}{r\partial\theta}\log(n_i + Zn_Z)\\ &+\frac{4}{3}\bar{\eta}_{0j}\frac{B^{3/2}}{m_j n_j}\hat{\mathbf{b}}\\ &\cdot\nabla\left\{\frac{\hat{\mathbf{b}}\cdot\nabla[(V_{\|j} + (B_\phi/B)\,\omega_j R)\,B^{1/2}]}{B^2}\right\}\\ &+\frac{T}{m_j}\frac{B}{\Omega_j}\frac{\partial\omega^{(0)}}{\partial r}\frac{1}{RB_\theta}\left(\frac{B_\phi}{B}\right)^2 R^2\hat{\mathbf{b}}\cdot\nabla\log n_j\\ &\pm\frac{m_i n_i}{m_j n_j}\nu_{iZ}D_{1i}(V_{\|i} - V_{\|Z}).\end{aligned} \tag{24}$$

In the right-hand side of (24) the physical meaning of the various terms is as follows: the first three terms describe inertial forces, the fourth the pressure driven force, the fifth the parallel electric field force, the sixth and seventh the parallel- ($\bar{\eta}_{0j}$ is defined in [14]) and gyro-viscous forces, respectively, and the last term, the friction force between ions and impurities, the sign of this term being plus for $j = Z$ and minus for $j = i$.

In order to avoid ambiguities two points have to be emphasized: (1) the set (23) and (24) does not exactly reproduce the first-order transient because the constitutive relationships giving the form of the viscous and friction forces come from steady state balances [1]; time dependence here is a computational artifice to get the steady state solution of a strongly nonlinear problem; (2) the set is correct only to $O(\delta_{pi})$, since it contains some but not all of the second-order terms. In particular, conservation laws cannot be satisfied to an accuracy better than first order (see [2] for details).

We finally notice that, rigorously, also $\omega^{(0)}$ evolves on the first-order time scale according to the first-order total flux surface averaged momentum balance in diamagnetic direction

$$\frac{d\omega^{(0)}}{dt} = \frac{1}{\sum_j m_j \langle R n_j \rangle} \times \left\{ \sum_j \left[ m_j \langle n_j \mathbf{V}_j \cdot \nabla \mathbf{V}_j \cdot \hat{\mathbf{e}}_\perp \rangle - \frac{B_\phi}{B} T \left\langle \frac{\partial n_j}{r \partial \theta} \right\rangle - \langle \nabla \cdot \boldsymbol{\Pi}_j^{(1)} \cdot \hat{\mathbf{e}}_\perp \rangle \right] - \frac{B_\phi}{B} T \left\langle \frac{\partial}{r \partial \theta} (n_i + Z n_Z) \right\rangle \right\}, \tag{25}$$

where $\boldsymbol{\Pi}_j^{(1)}$ is the first-order viscous stress tensor obtained i [1]. This equation is solved in the code as well, in order t check that the total axial angular momentum be conserve to first order. However, the physically significant evolutio of $\omega^{(0)}$, which is driven by the momentum source, tak place only on the second-order time scale.

The driving force for the first-order evolution is the ior impurity friction, which appears now, due to the specie dependence of $\omega_j^{(1)}$. The latter depends on the radi gradients of the zeroth order densities and rotatio frequency; these gradients are presently taken as give quantities, since the radial profiles evolve as seen only o the slowest, second-order time scale.

Space discretization of the system (23)–(25) is accon plished by means of a Fourier pseudo-spectral metho [15], taking advantage of the periodicity in poloidal angl Typically, 16 to 32 points in $\theta$ are sufficient to g reasonably accurate results (see next section); this numb increases when one goes from intermediate to large Mac numbers.

To assess the problem associated with the time integra tion of the resulting system of ordinary differential equa tions (ODE), the eigenvalues of the evolution operator hav been computed numerically, for poloidal profiles typicall used as initial condition and parabolic radial profiles, usin the NAG [16] routines F01ATF, F01AKF, and F02API From the plot shown in Fig. 4 one sees that the system i stiff, with very large, purely real, negative eigenvalue which are superimposed to the usual pattern of an advec tion/diffusion problem, dominated by advection in our cas In particular, numerical experiments [2] show that i absolute value the largest eigenvalues decrease almo proportionally when the ion-impurity friction force i

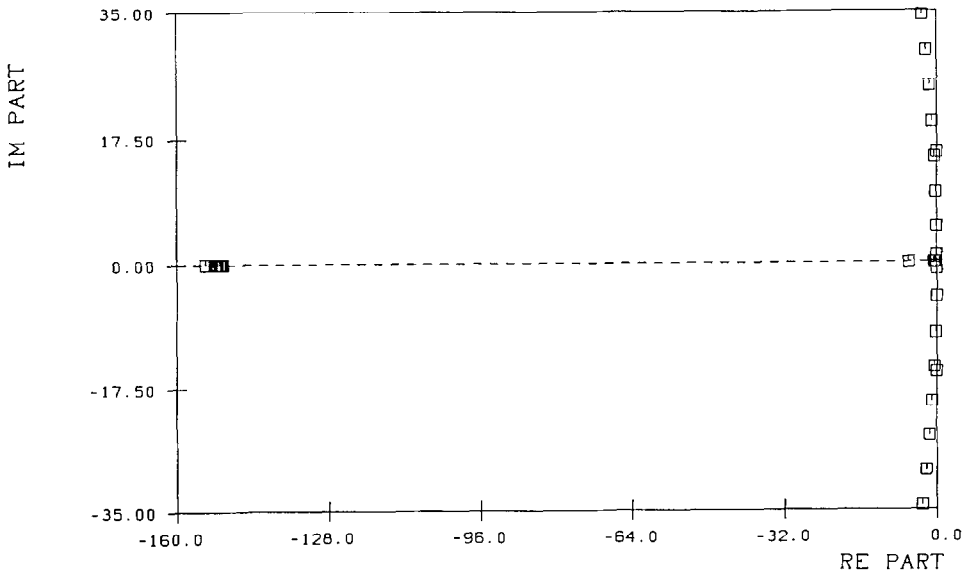


**FIG. 4.** Poloidal Jacobian eigenvalues. Location in the complex plane (Re $\beta_k$, Im $\beta_k$) of the eigenvalues $\beta_k$ of the first-order evolution operato obtained at $t = 0$ by pseudospectral discretization in $\theta$; parabolic radial profiles are assumed.

artificially reduced. Due to its stiffness, the system of ODE resulting from space discretization of (23)–(25) is solved by the NAG [16] routine D02EAF, implementing Gear's method [17].

### 4.2. *Results*

Unless noted otherwise, the values of the parameters used for solution are the same as in the zeroth-order case. As compared to average plasma conditions in present tokamak experiments a very low temperature (we choose $T = 35$ eV) is required in order to have both ions and impurities well in the Pfirsch–Schlüter regime. The ion transit time turns out to be $\tau_t \approx 30\ \mu$s, the ion–ion collision time $\tau_{ii} \approx 10\ \mu$s, and $\delta_{pi} \approx 10^{-2}$.

We take as initial poloidal density profiles those corresponding to the zeroth order steady state, while the initial parallel flow velocities correspond to zero poloidal flow and given radial gradients of the average densities and rotation frequency. In the example discussed in this section, the average ion density and average rotation frequency radial profiles are parabolic, and both vanish at the boundary; in the center, $\bar{n}_i = 8.0 \times 10^{19}\ \mathrm{m}^{-3}$ and MACH $= 1$; everywhere in radius $\bar{\alpha} = 1$.

As representative of the first-order evolution, the dependence on time of

$$K_j^{(1)}(r) \equiv \left\langle \frac{n_j V_{\theta j}}{B_\theta} \right\rangle \frac{B_{\theta 0}}{\bar{n}_j} \tag{26}$$

is given in Fig. 5 normalized to $\delta_{pi} v_{thi}$, where the dashed line refers to the ions and the solid one to the impurities. One sees that a steady state characterized by nonzero ion and impurity poloidal flows is reached after some $\tau_t/\delta_{pi}$.

The steady state poloidal profiles of ion (dashed line) and impurity (solid line) density, normalized to the respective $\bar{n}_j$, and of the difference between ion and impurity toroidal flow velocities, normalized to $\delta_{pi} v_{thi}$, are shown in Fig. 6. One sees that when the first order evolution has reached steady state, toroidal ion-impurity friction drives up–down asymmetries in the density distribution. The asymmetry turns out to be only $O(\delta_{pi})$ as expected; still it is very important for radial transport as discussed in the next section.

In the absence of first-order sources, and of radial transport to this order, the number of particles for each ion species and the total axial angular momentum must be conserved on each surface during the evolution. The relative errors resulting from the present computation are $< 10^{-9}$ and $< 10^{-3}$, respectively [2]. The steady state results of the first-order evolution were also shown in [20] to be in good agreement with those obtained for the static case using the same physical model, but a completely different analytical method [1] which is then evaluated numerically.

Taking again $O^{2+}$ as impurity species, instead of $O^{6+}$, it was shown elsewhere [2, 22] that the amplitude of the first-order modulations grows with $\zeta$ and their spectrum changes.

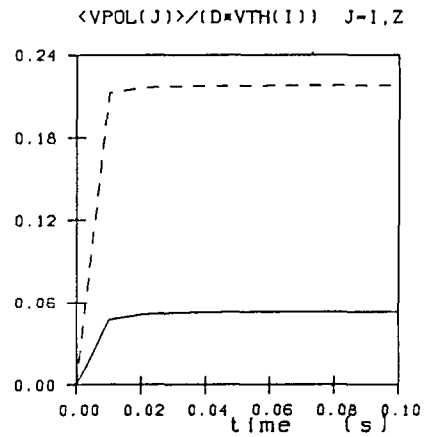


**FIG. 5.** First-order evolution to steady state: ion (dashed line) and impurity (solid line) flux surface averaged poloidal particle flows $K_j^{(1)}$, normalized to $\delta_{pi} v_{thi}$, vs time.

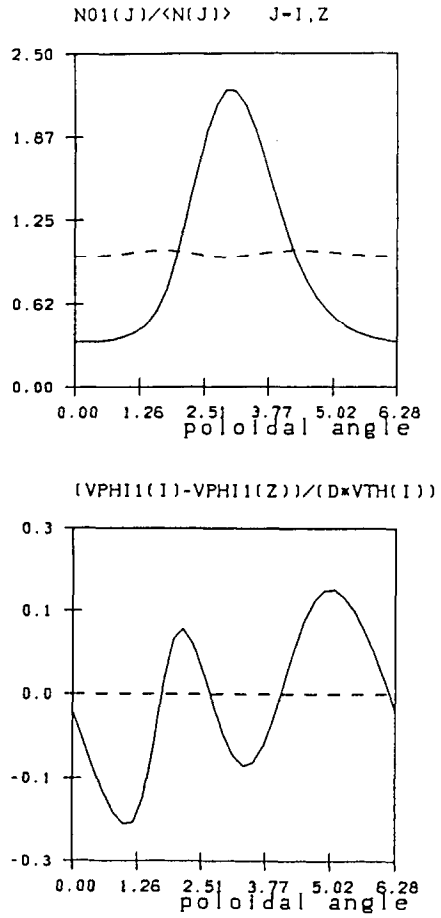


**FIG. 6.** Steady state profiles after relaxation of the first-order evolution, as a function of poloidal angle $\theta$. Above: $n_i/\bar{n}_i$ (dashed line), $n_Z/\bar{n}_Z$ (solid line); below: $(V_{\phi i} - V_{\phi Z})/v_{thi}$.

## 5. EVOLUTION ON THE SECOND-ORDER TIME SCALE

### 5.1. *Radial Equations*

The equations which describe the evolution of the radial profiles of the flux quantities $\bar{n}_j$ and $\omega^{(0)}$ on the slow second-order time scale are the flux surface averaged continuity equations for the main ions and the impurities, and the total (i.e., summed over species) flux surface averaged axial angular momentum balance.

In the case of Pfirsch–Schlüter collisionality, constant uniform temperature, fixed circular concentric magnetic surfaces, these equations can be written [1, 2]

$$\frac{\partial \langle n_j^{(0)} \rangle}{\partial t_2} = \frac{1}{eZ_j} \frac{1}{rR_0} \frac{\partial}{\partial r} \times \left( \frac{r}{B_{\theta 0}} \langle RF_{\phi j}^{(1)} \rangle \right) + \langle S_j \rangle \tag{27}$$

$$\frac{\partial}{\partial t_2} \left( \sum_j m_j \langle Rn_j^{(0)} V_{\phi j}^{(0)} \rangle \right) = \frac{1}{rR_0} \frac{\partial}{\partial r} \left( \frac{r}{B_{\theta 0}} \omega^{(0)} \sum_j \frac{B}{\Omega_j} \langle R^3 F_{\phi j}^{(1)} \rangle \right) + \sum_j \langle RM_{\phi j} \rangle, \tag{28}$$

where $j = i$, $Z$ is the species index, the upper indexes in parentheses refer to the order in $\delta_{pi}$,

$$F_{\phi i}^{(1)} = -F_{\phi Z}^{(1)} = m_i n_i \nu_{iZ} D_{1i} (V_{\phi Z} - V_{\phi i}) \tag{29}$$

is the first-order toroidal friction, $D_{1i}$ is a coefficient of $O(1)$ given in [1], $S_j$ is the (second-order) particle source, and $M_{\phi j}$ is the (second-order) toroidal momentum source. The poloidal magnetic field $B_{\theta 0} = (R/R_0)\, B_\theta$ will be assumed in the following to vary linearly with $r$, only for the sake of simplicity; this corresponds to circular concentric equilibria with parabolic pressure profiles, neglecting the para- or dia-magnetism of the plasma.

We observe that thanks to the assumption of uniform temperature there is no thermal force [3] contribution to the friction in (29); for the purpose of later reference we also recall that it is customary [11] to decompose the toroidal friction into two components

$$F_{\phi j}^{(1)} = \frac{B_\phi}{B} F_{\| j}^{(1)} - \frac{B_\theta}{B} F_{\perp j}^{(1)}; \tag{30}$$

the radial transport coming from the perpendicular (diamagnetic) component is called *classical*, and that coming from the parallel one, *neoclassical*.

Probably the most striking feature of the radial set of equations is the fact that, within the limits of the previously mentioned simplifying assumptions, the neoclassical radial flux of axial angular momentum has no explicit viscosity contribution. This results from an exact cancellation between the stress tensor contribution proper and the part of the convective contribution which comes from the viscous force (see [2] for details). This does not mean, however, that the momentum flux is, strictly speaking, purely convective, because it is generally not simply proportional to the particle flux (see (46) and related discussion).

Using the zeroth order solution of Section 3 the radial transport equations can be rewritten as

$$\frac{\partial \bar{n}_j}{\partial t_2} = \frac{b}{Z_j} \frac{1}{r} \frac{\partial}{\partial r} (\langle RF_{\phi j}^{(1)} \rangle) + \langle S_j \rangle \tag{31}$$

$$\frac{\partial}{\partial t_2} \left( \omega^{(0)} \sum_j m_j \bar{n}_j \frac{\langle R^2 A_j^{(0)} \rangle}{\langle A_j^{(0)} \rangle} \right) = -\frac{c}{r} \frac{\partial}{\partial r} (\omega^{(0)} < R^3 F_{\phi i}^{(1)} \rangle) + \sum_j \langle RM_{\phi j} \rangle, \tag{32}$$

where

$$b \equiv \frac{q}{eB_\phi}, \qquad c \equiv (\zeta - 1) \frac{q}{\Omega_i}, \tag{33}$$

and $q \equiv rB_\phi / RB_\theta$ is the safety factor.

One can notice from (32) and (33) that the model contains an isotope effect: in a deuterium plasma with a single fully ionized impurity species $c = 0$, so that the only mechanism left for the radial transport of the axial angular momentum is classical perpendicular viscosity, which is neglected here because it is small; this is an interesting feature of the model, since in deuterium plasmas rotation velocities have been measured [6] to be larger—i.e., the momentum to be better confined—than in hydrogen, for the same injected power.

Since it is convenient for the numerical solution to keep the radial system in the form of conservation laws, we choose as unknowns the two densities $\bar{n}_j$ and the total axial angular momentum

$$\mathscr{P}_\phi \equiv \omega^{(0)} \sum_j m_j \bar{n}_j \frac{\langle R^2 A_j^{(0)} \rangle}{\langle A_j^{(0)} \rangle}. \tag{34}$$

During the solution process one needs, however the evolving value $\omega^{(0)}(t)$, which depends through (34) non-linearly on $\mathscr{P}_\phi$ (recall from Section 3, Eq. (12), that $A_j^{(0)}$ depends on $\omega^{(0)}$ both explicitly and implicitly). After each step of the second-order time integration $\bar{n}_j$ and $\mathscr{P}_\phi$ are

known, and to determine $\omega^{(0)}(t)$ a double iteration is performed [2]: the inner one uses the algorithm for the zeroth-order solution, starting with given $\bar{n}_j$ and tentative $\omega^{(0)}$, and relaxes to some $A_j^{(0)}$; then, in the outer iteration, a new $\omega^{(0)}$ is determined from this solution and the given $\mathscr{P}_\phi$, using (34), and the process is repeated until convergence is reached.

For the forthcoming discussion we define

$$H^{(1)} \equiv \langle RF_{\phi i}^{(1)} \rangle \propto \Gamma_Z, \qquad G^{(1)} \equiv \langle R^3 F_{\phi i}^{(1)} \rangle \propto \Gamma_\omega, \tag{35}$$

where $\Gamma_Z$ is the impurity radial particle flux, and $\Gamma_\omega$ the total radial flux of axial angular momentum. The set of radial equations to be discretized is then

$$\frac{\partial \bar{n}_i}{\partial t_2} = b \frac{1}{r} \frac{\partial H^{(1)}}{\partial r} + \langle S_i \rangle \tag{36}$$

$$\frac{\partial \bar{n}_Z}{\partial t_2} = -\frac{b}{Z} \frac{1}{r} \frac{\partial H^{(1)}}{\partial r} + \langle S_Z \rangle \tag{37}$$

$$\frac{\partial \mathscr{P}_\phi}{\partial t_2} = -\frac{c}{r} \frac{\partial}{\partial r} (\omega^{(0)} G^{(1)}) + \sum_j \langle RM_{\phi j} \rangle. \tag{38}$$

Another feature of the model is by now apparent: multiplying the continuity equations by the respective charges and summing them together one obtains, as a result of ambipolarity in particle transport

$$\frac{\partial}{\partial t} (\bar{n}_i + Z\bar{n}_Z) = \sum_j Z_j \langle S_j \rangle. \tag{39}$$

From (39) one observes that: first, the system can be reduced to two PDE for $\mathscr{P}_\phi$ and, say, $\bar{n}_Z$, whereas the ion density is given at any time by

$$\bar{n}_i(r, t) = \bar{n}_i(r, 0) + Z(\bar{n}_Z(r, 0) - \bar{n}_Z(r, t)) + \int_0^t \sum_j Z_j \langle S_j \rangle \, dt; \tag{40}$$

second, in order to get a steady state in our model the right-hand side in (39) must be zero (at least from a given time on), and we shall assume for the sake of simplicity that at any time

$$\langle S_i \rangle = \langle S_Z \rangle = 0. \tag{41}$$

Notice that this is essentially a limitation of our model: collisions with electrons, which we neglect here, could in fact transport particles out of the plasma, ambipolarly, relaxing the need to impose (41); however, as seen in Section 1, this would happen only on a time scale longer than second order by a factor $O(\sqrt{m_i/m_e})$, i.e., too slow for being of any practical interest.

### 5.2. *Boundary Conditions*

The set of radial equations, for the vector of the unknowns $\Xi \equiv (\bar{n}_Z, \mathscr{P}_\phi)$, still has to be supplemented by suitable initial and boundary conditions. As the initial condition we usually take simple parabolic profiles in the radial direction. The question of the boundary conditions is rather delicate, as we will see below.

The fluxes $H^{(1)}$ and $G^{(1)}$ depend themselves on radial gradients, so that the radial evolution described by (36)–(38) is parabolic in nature. Notice, however, that this does not mean conventional diffusive behavior where any initial profile tends to flatten out in the absence of sources. In our case, whenever one of the two ion species flattens out the other does in fact peak as a result of ambipolar particle transport [4].

On the magnetic axis we impose zero fluxes:

$$H^{(1)}|_{r=0} = 0, \qquad G^{(1)}|_{r=0} = 0 \tag{42}$$

(note that this is not strictly speaking a boundary condition, but rather a constraint on the regularity of the sources).

At $r = a$ (plasma minor radius) we could in principle impose either Dirichlet (on $\Xi$) or Neumann (on $H^{(1)}$ and $G^{(1)}$) conditions, or else a combination of the two. Let us consider first the case of Dirichlet boundary conditions. From a physical point of view they are difficult to justify, at least for the density, because there seems to be no obvious direct way to maintain it at a prescribed value at the plasma edge. Furthermore, the particle fluxes at the boundary are now free to adjust themselves, and due to ambipolarity they will be either both trivially zero, or in opposite directions; in the latter case, during the transient, one of the two ion species would flow incontrollably through the boundary into the plasma: one would eventually reach some steady state, characterized by zero particle fluxes, although not a physically significant one, since it would assume the availability of either fuel or impurities to feed the plasma from outside. One could still in principle impose a Dirichlet condition on $\omega^{(0)}$ at the boundary, but the actual implementation of this condition would be problematic due to our choice of the radial grid and of the other boundary conditions (see also the next section). Furthermore, information related to the physical mechanism which slows down the plasma rotation near the boundary can be more readily included in the model using a mixed (Robin) type boundary condition, as we are going to see.

In view of the difficulties just mentioned we impose Neumann boundary conditions on the density and a mixed boundary condition for the evolution of $\mathscr{P}_\phi$.

Integrating the impurity continuity equation over the whole plasma volume one sees that in the absence of particle sources the condition to get steady state is that

$$H^{(1)}|_{r=a}=0, \tag{43}$$

at least from a given time on, and we will impose this condition for all times.

The physics of the radial set just described is not necessarily valid near a limiter or separatrix, where sources and sinks could possibly appear already to the first order, as opposed to the case treated here where they enter only the slow second-order evolution. Therefore we assume for simplicity that in the boundary region the radial transport of axial angular momentum be proportional to the toroidal rotation frequency; that is,

$$(\omega^{(0)}G^{(1)})|_{r=a}=\lambda\omega^{(0)}|_{r=a}. \tag{44}$$

This is equivalent to assuming some form of aerodynamic drag opposing rotation near the boundary, and for this process a number of physical mechanisms have been suggested in the past, for instance, charge-exchange.

For our present purposes the value of $\lambda$ can be chosen subject to the constraint that the numerically determined momentum confinement time $\tau_\phi$ not be strongly sensitive to this choice (see Section 5.4 for further discussion). In order to quantify this requirement, we considered the solution of an analogous simplified problem [18], together with the assumption that the radial momentum flux is proportional to the effective viscosity given in [19]: the relevant inequality that must be satisfied by $\lambda$ is found to be [2], in SI units,

$$\lambda>0.25. \tag{45}$$

This restriction corresponds physically to the requirement that the prescribed transport coefficient at the boundary is larger than the average coefficient in the inner region.

We conclude the discussion of the boundary conditions noting that we have imposed the homogeneous condition (44) in the driven, inhomogeneous problem (38). This is advisable because an inhomogeneous condition would make the steady state solution strongly dependent on the initial condition.

### 5.3. *Numerical Method and* 1 + 1 D *Algorithm*

From the computational physics point of view the essential difference between the cases of negligible and strong rotation consists in the fact that, while in the former the radial fluxes are explicit functions of the quantities evolving on the second-order time scale [4], in the latter this dependence is an implicit one. In fact, the particle and angular momentum radial fluxes are driven by the first-order toroidal friction. The analysis of the problem on the first-order time scale in Section 4 has shown that the driving force giving rise to a nonzero toroidal friction comes from two contributions, proportional to $\partial\omega^{(0)}/\partial r$ and $(\partial/\partial r)\log(\bar{n}_j/\langle A_j\rangle)$, respectively. To make the computation self-consistent these gradients have to be determined from the solution of the radial problem, so that the following procedure is employed.

Thanks to the separation of time scales, one can assume the radial gradients to be constant during the $O(\delta_{pi})$ evolution. On the other hand, the radial gradients will change during the $O(\delta_{pi}^2)$ evolution, so that one will need to recompute the first-order equilibria on the surfaces in order to update the toroidal friction in the radial equations.

The explicit dependence of $H^{(1)}$ and $G^{(1)}$ on $\bar{n}_j$ and $\omega^{(0)}$ being unknown, one has to compute the radial derivatives on the right-hand sides of the radial system by solving the first-order poloidal problem on several magnetic surfaces.

We choose to solve the radial set with the method of lines. Since both the first- and the second-order unknowns evolve due to radial gradients of quantities evolving on the *other* time scale, it is natural to discretize the radial coordinate on two staggered equidistant meshes as shown in Fig. 7: a *fluxes* mesh $\mathcal{M}_1$, where $H^{(1)}$ and $G^{(1)}$ are collocated, with $m$ points, the first and last of which at $r=0$ (magnetic axis)

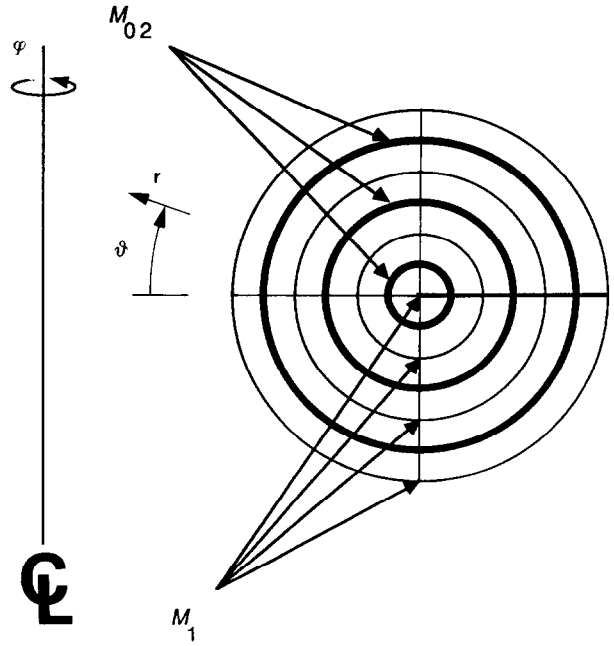


**FIG. 7.** The 2D $(r,\theta)$ mesh: the poloidal angle is uniformly discretized; in radius two staggered equidistant meshes are used. The zeroth and second-order calculations are performed on $\mathcal{M}_{02}$, the first order on $\mathcal{M}_1$.

and $r = a$ (plasma ideal surface), respectively; a *values* mesh $\mathcal{M}_{02}$, where $\Xi$ is collocated, with $m1 \equiv m - 1$ points, the first of which half the way between the first two points of $\mathcal{M}_1$. The radial derivatives are discretized by second-order accurate finite differences, but the overall space accuracy of the scheme is only first order, because linear interpolation is used to map from one mesh to the other.

There is no way to step forward the radial equations implicitly in time because, as already pointed out, the explicit dependence of the fluxes on $\Xi$ is unknown. On the other hand, one must try to couple, as much as possible, the computations on the first- and second-order time scales, if the right-hand side in the radial set has to describe a diffusion-like operator and not a pure source term.

The choice of the algorithm for the time integration of the

require a very stringent time accuracy; this would in fact increase disproportionately the number of first-order steady states that need be computed, which is the most expensive portion of the scheme.

In view of the points mentioned the choice is basically restricted to predictor–corrector and Runge–Kutta methods. We use a second-order explicit predictor–corrector "PC2" with first-order predictor and second-order corrector, or a fourth-order explicit Runge–Kutta–Merson "RKM4." Both of the methods allow a control of the local truncation error, and require two and five right-hand side evaluations, respectively.

Due to the low relative accuracy required ($\approx 10^{-3}$) and to similar stability regions, the two methods are found to perform comparably for this problem, in terms of the CPU time required to obtain a steady state on the second-order time scale.

The time step size is adapted internally: for a given required accuracy ("TOL"), the local truncation error ("ERR") is computed after each step. If ERR > TOL the step is rejected and $\Delta t$ is halved; if TOL1 < ERR < TOL, $\Delta t$ is kept constant, and if ERR < TOL1 for more than $k+1$ steps [17], $\Delta t$ is doubled. The relative error bound "TOL1" that we use is TOL1 = TOL/10, TOL/50 and $k = 2, 4$ for PC2 and RKM4, respectively; note that one needs TOL1 < TOL/$2^{k+1}$ not to have to halve the step right after having doubled it.

Since the required accuracy is not very stringent, the stability threshold of the method is quickly reached; if at some point the step has to be halved after having already been doubled previously, the eigenvalues of the Jacobian of the radial set are determined numerically, and the new $\Delta t$ fixed according to an almost marginal stability criterion [2]. No further increase of $\Delta t$ is allowed in this case, i.e., we assume that the Jacobian eigenvalues do not significantly vary any more before the system reaches steady state; this is verified a posteriori in most instances.

For the 2D problem dealt with in this paper we propose a 1 + 1 D algorithm, which can now be summarized as follows:

- Initialize $\Xi$ on $\mathcal{M}_{02}$;
- Compute the zeroth order steady state on $\mathcal{M}_{02}$, and determine the $A_j^{(0)}$ from the result {(16), (17)};
- Determine $\partial\omega^{(0)}/\partial r$ and $(\partial/\partial r)\log(\bar{n}_j/\langle A_j^{(0)}\rangle)$ on $\mathcal{M}_1$, and interpolate $\Xi$ from $\mathcal{M}_{02}$ to $\mathcal{M}_1$;
- Compute the first-order evolution on $\mathcal{M}_1$ {(23)–(25)}, and determine $H^{(1)}$ and $G^{(1)}$ from the result;
- Impose the boundary conditions on $\mathcal{M}_1$ {(42)–(44)};
- Determine $\partial H^{(1)}/\partial r$ and $\partial\omega^{(0)}G^{(1)}/\partial r$ on $\mathcal{M}_{02}$;
- Obtained the updated $\Xi$ on $\mathcal{M}_{02}$ by stepping forward in time the radial equations {(37), (38)};

second-order time scale.

### 5.4. *Results*

We describe in the following a few representative results of the 1 + 1 D computation, showing the evolution to steady state of the radial profiles of ion and impurity surface averaged density $\bar{n}_j$ and lowest order toroidal rotation frequency $\omega^{(0)}$. Cases with and without momentum sources acting on the plasma will be considered. The method PC2 was used for time integration. A comparison with the theoretical results [4] in the case of negligible rotation is given in [2], where excellent agreement was found with the results of our code. Results of convergence tests are also given in [2].

The initial condition is, unless noted otherwise,

$$\bar{n}_i(r) = 8.0\times 10^{19}[1-(r/a)^2] + 8.0\times 10^{19}\ \mathrm{m}^{-3},$$
$$\bar{\alpha}(r) = 1,$$
$$\mathrm{MACH}(r) = 0.5[1-(r/a)^2],$$

and we use a $5\times 16$ mesh in the $(r,\theta)$ plane. For the parameters whose values have not been previously specified we take: $B_{\phi 0} = 2.5$ T, $B_{\theta 0}(r) = 0.366(r/a)$ T, $R_0 = 1.64$ m, $a = 0.4$ m.

We consider first a case without momentum source ($M_{\phi j} = 0$). The boundary conditions are here zero particle and momentum ($\lambda = 0$) fluxes, i.e., the plasma is an isolated system. During the second-order evolution to steady state, the total number of ions, $\propto \int_0^a \bar{n}_i r\,dr$, the total number of impurities, $\propto \int_0^a \bar{n}_Z r\,dr$, and the sum of the ion and impurity axial angular momentum, $\propto \int_0^a \mathcal{P}_\phi r\,dr$, are conserved with a relative error smaller than $10^{-12}$ [2].

The initial (dash-dotted line) and steady state (solid line) radial profiles of $\bar{n}_i$, $\bar{n}_Z$, and MACH are shown in Fig. 8a as

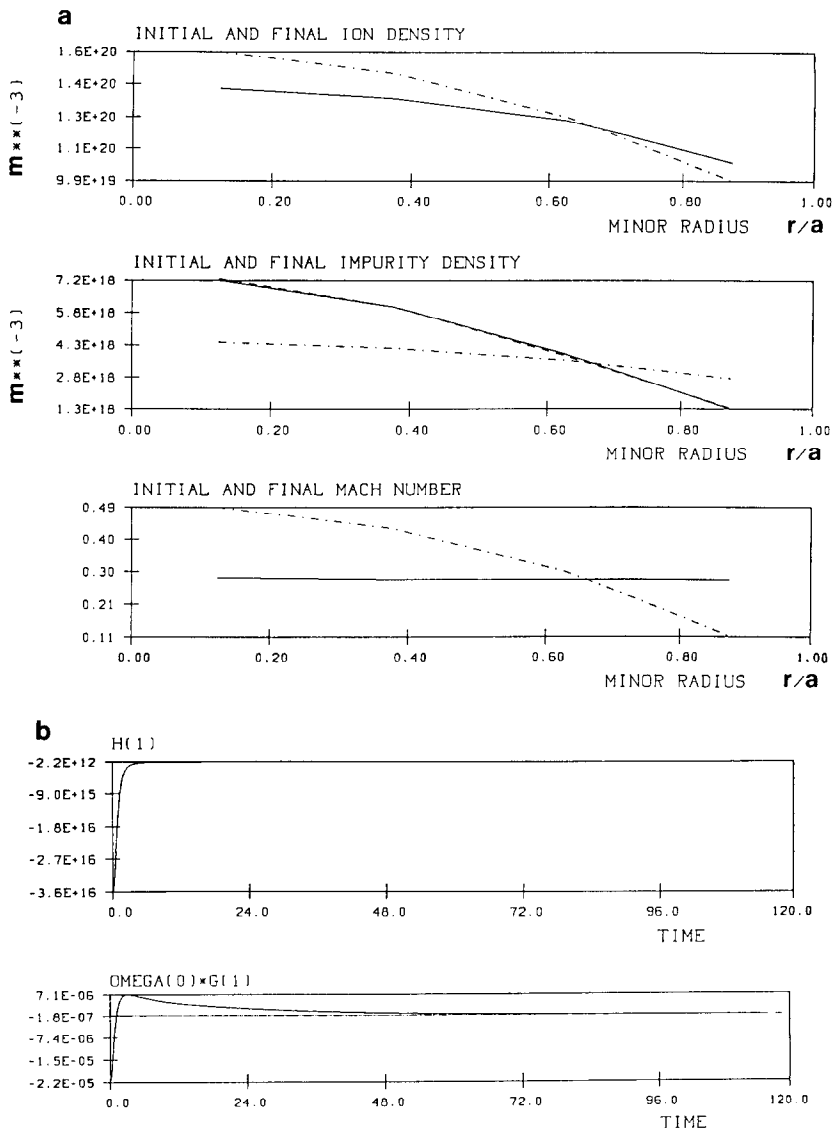


**FIG. 8.** (a) Second-order evolution in the absence of sources: $\mu = 0$, $\lambda = 0$. Initial (dash-dotted line) and steady state (solid line) radial profiles of $\bar{n}_i$, $\bar{n}_Z$, and MACH. The dashed line is the theoretically foreseen profile for the nonrotating case [4]. (b) Second-order evolution in the absence of sources: $\mu = 0$, $\lambda = 0$. Radial impurity particle flux $\Gamma_Z$ (above) and total axial angular momentum radial flux $\Gamma_\omega$ at $r = a/2$ vs. time (the dashed line corresponds to vanishing flux, the dotted to the exact steady state).

a function of the normalized minor radius $r/a$. One notes that the impurities tend to peak in the center and the ions correspondingly to flatten. The dashed line indicates here (and in the similar plots that will follow) the profile containing the same total number of impurities as the obtained $\bar{n}_Z$ profile, and following the obtained $\bar{n}_i(r)$ normalized profile to the $Z$th power: the latter radial dependence is the neoclassical prediction for the impurity profile in the nonrotating case [4]. One sees that in our case the steady state profile of the rotation frequency is flat: since the Mach number enters the driving force of the first-order evolution only through gradients, it has to be expected that the density profiles should be in this case the same as in a nonrotating plasma. The fact that the rotation frequency becomes homogeneous in radius is also intuitive if one remembers that in a pure, slowly rotating plasma [19] the momentum flux is simply proportional to the gradient of the rotation velocity: the gradient must then go everywhere to zero at steady state, when the system is isolated and there are no momentum sources; the level of the uniform rotation frequency will be determined by the initial condition through conservation of the total axial angular momentum. (Since the particle fluxes depend on the combination of ion and impurity density gradients, even in the absence of particle sources the system generally does not run towards flat density profiles at steady state).

To prove that one actually reaches steady state, in Fig. 8b we show the computed impurity particle- and axial-angular momentum radial fluxes through the surface located at $r = a/2$ vs. time. It is interesting to note from these plots that the momentum flux apparently consists of two contributions: one, which we could call convective, essentially following the particle flux; another, which we could call conductive (or pseudo-viscous), going to zero on a slower time scale. Recalling (35) this behavior can be related to the fact that, due to the poloidal variation of ion-impurity friction,

$$\langle R^3 F_\phi^{(1)} \rangle = R_0^2 \langle R F_\phi^{(1)} \rangle + \text{other terms.} \tag{46}$$

We finally notice that, comparing the effective viscosity given in [19] (which, however, applies strictly speaking only to a pure, slowly rotating plasma) with the diffusion coefficient in [4], the fact that $\Gamma_Z$ and $\Gamma_\omega$ do not evolve on the very same time scale is not unexpected.

We consider now the evolution of the system subject to the action of a momentum source. The source is distributed over the plasma cross section according to

$$\sum_j M_{\phi j}(r, \theta) \equiv \mu \left(1 - \left(\frac{r}{a}\right)^2\right)^\delta, \qquad \delta = 0, 1, \tag{47}$$

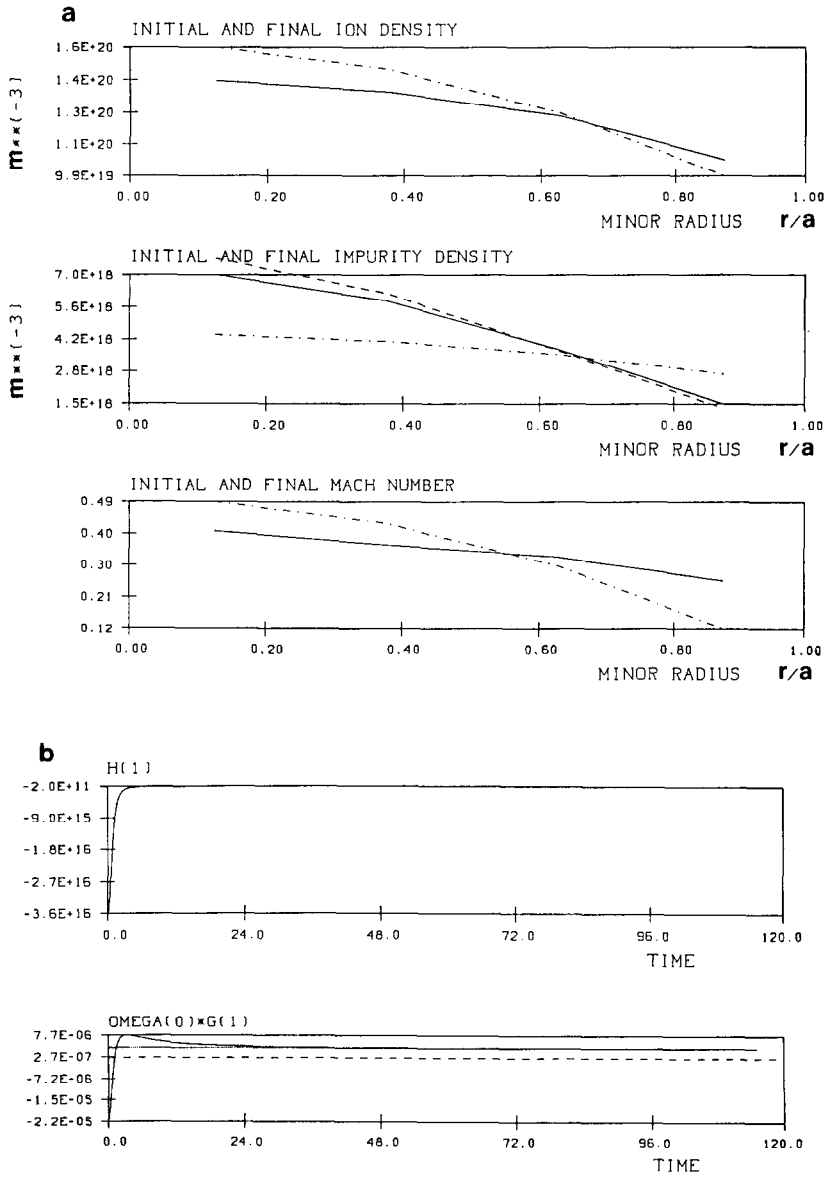


**FIG. 9.** (a) Effect of momentum source: same parameters as in Fig. 8a, except $\mu = 10^{-4}$, $\lambda = 0.3$. (b) Effect of momentum source: same parameters as in Fig. 8b, except $\mu = 10^{-4}$, $\lambda = 0.3$.

so that, by analytic integration of (38) in $r$, and using (44), one obtains the rotation frequency at the plasma boundary at steady state,

$$\omega^{(0)}|_{r=a} = \frac{\mu}{\lambda}\frac{a^2 R_0}{c} s_\delta, \tag{48}$$

where $s_0 = \frac{1}{2} + \frac{1}{8}(a/R_0)^2$, $s_1 = \frac{1}{4} + \frac{1}{24}(a/R_0)^2$. In the following results a uniform source is used, i.e., $\delta = 0$. (Note that the simple form chosen for the source also allows us to determine analytically the steady state radial profile of $\omega^{(0)}G^{(1)}$ and therefore to check the numerical result: in the case $\delta = 0$, e.g.,

$$\Gamma_\omega(r) = \frac{R_0}{2c}\left[1 + \left(\frac{r}{2R_0}\right)^2\right] r^2, \tag{49}$$

so that, for instance, $\Gamma_\omega(r = a/2)$ must be equal to $\frac{1}{4}\Gamma_\omega(r = a)$.)

Equation (48) is used in the following way: one chooses a source intensity $\mu$ giving (by numerical experiment) a central Mach number in the range we are interested in (say $0.4 < \mathrm{MACH} < 0.8$); the value of $\lambda$ is then chosen such that a reasonably low Mach number at the boundary is obtained at steady state. This $\lambda$ should finally also satisfy the constraint (45). We remark, however, that a very large $\lambda$ requires us to discretize the region near the boundary with many points in $r$; otherwise an artificially negative MACH($a$) is obtained.

evolution is to compare the Mach numbers obtained at tl boundary in different cases. Notice, when comparing tl following results among themselves, that the Mach numb is discretized on $\mathcal{M}_{02}$, whereas the physical boundary ($r =$ belongs to $\mathcal{M}_1$. The Mach number at the boundary obtained from the result of the code by linear extrapolatic

$$\mathrm{MACH}(a) \equiv \mathrm{MACH}(r_m^{(1)}) \approx \tfrac{3}{2}\mathrm{MACH}(r_{m-1}^{(02)}) - \tfrac{1}{2}\mathrm{MACH}(r_{m-2}^{(02)}). \tag{5}$$

In Fig. 9a we show the initial and steady state radi profiles, for the case $\mu = 10^{-4}$, $\lambda = 0.3$ (SI units). Or notices that the presence of a momentum source results in nonflat MACH profile at steady state; this in turn leads density profiles which are sensibly different from tho predicted for a nonrotating plasma. As before, we prove tl attainment of steady state showing in Fig. 9b the impuri particle- and total axial-angular momentum radial fluxes $r = a/2$ vs. time. While $\Gamma_Z$ still goes to zero (no particle sou ces are present), $\Gamma_\omega$ at steady state balances the momentu input in the volume $r < a/2$. The dotted line represents tl exact analytical steady state value which obtains from (49

In Fig. 10 the corresponding radial profiles obtained the case $\mu = 10^{-4}$, $\lambda = 0.6$ are given. At steady sta MACH($a$) turns out to be (with a 2% relative error) ha that for the case $\mu = 10^{-4}$, $\lambda = 0.3$, as expected. The chara teristic times for the second-order evolution are n apparently influenced by the change in $\lambda$ [2].

Finally, the radial profiles for the case $\mu = 2 \times 10^{-}$

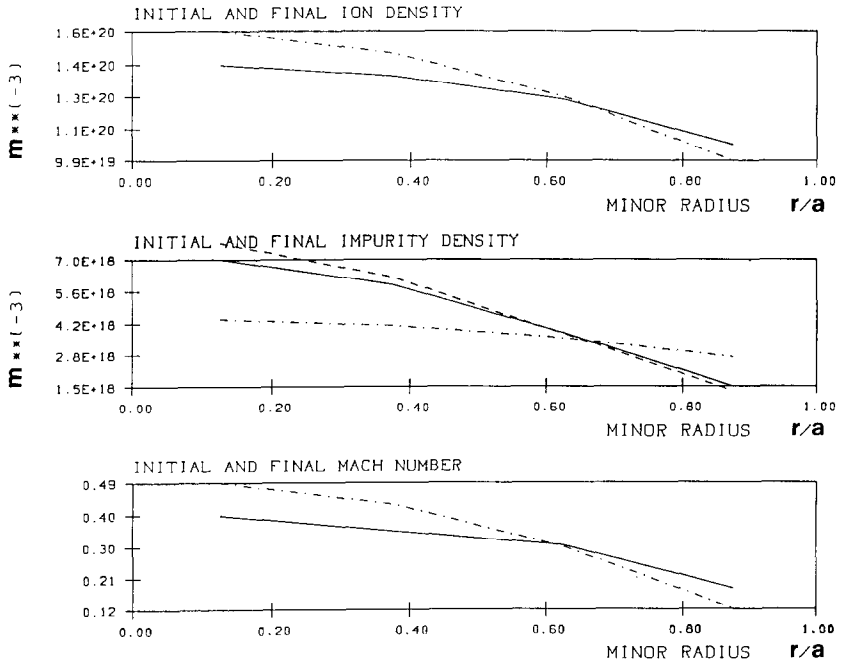


**FIG. 10.** Same as Fig. 9a, except $\lambda = 0.6$.

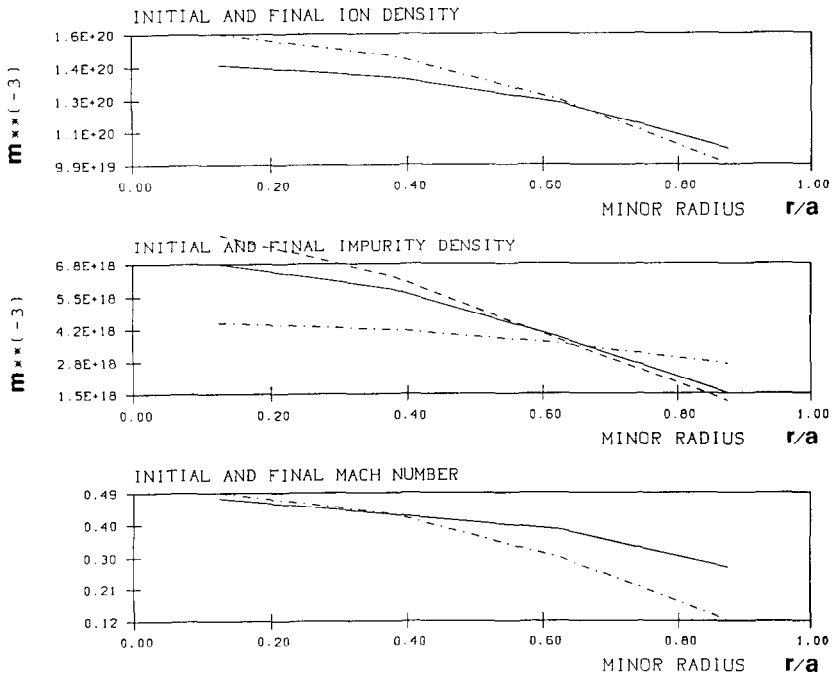


**FIG. 11.** Same as Fig. 9a, except $\mu = 2 \times 10^{-4}$, $\lambda = 0.6$.

same (with a less than 1% relative error) as those for the case $\mu = 10^{-4}$, $\lambda = 0.3$, as it must be, since the ratio $\mu/\lambda$ is the same. Having doubled the source intensity, compared to the case of Fig. 9a, results in a less than proportional increase of the central Mach number, indicating that the momentum source/toroidal flow relationship is nonlinear.

## 6. CONCLUSION

In this paper we have considered the two-dimensional, multiple time scale problem of particle and momentum transport in a strongly rotating tokamak plasma constituted by electron, fuel ion, and a single impurity ion species.

An algorithm has been presented that is capable of reducing the full 2D problem to an alternation of 1D problems. The steady state distributions of the relevant plasma parameters, resulting from the evolution on each of the (three) separate time scales, have been computed numerically from a multifluid model [1].

On the zeroth-order time scale the impurity density on each magnetic surface is strongly peaked outboards due to inertial forces, and the rotation on each surface is purely rigid toroidal and common to all species.

On the first-order time scale up–down asymmetries appear in the poloidal distribution of the densities, due to ion-impurity toroidal friction; the latter results from species dependent diamagnetic flow which is related to radial gradients of density and rotation frequency, and these are taken as given constant in time functions at this stage. Nonzero poloidal flows of ions and impurities are obtained at steady state.

On the second-order time scale the evolution of the radial profiles takes place, driven by sources and by fluxes depending on the toroidal friction; after each time step of the second-order evolution the first order can then be recomputed using the new radial gradients, and the resulting toroidal friction is then used in the subsequent step of the second-order computation.

When the plasma is isolated, the radial profile of the toroidal rotation frequency becomes flat after the second-order evolution has relaxed to steady state; i.e., the whole plasma rotates as a rigid body. The radial profile of the densities is the same as in the absence of rotation.

When the plasma is subject to a momentum source, radial gradients in the rotation frequency profile can be maintained at steady state, and the densities distribution is different from the nonrotating case.

In both driven and nondriven problems the evolution of the radial profile of toroidal rotation frequency has been shown to follow the densities in its first stage, but then to reach steady state only at a later time.

Some requirements of the present model, in particular the large plasma collisionality and the constant uniform temperature assumed, have to be relaxed before a comparison with experimental results becomes meaningful (the problem of the energy balance in a rotating plasma has been recently addressed in [21]). Our purpose here was to propose a computational method based on a physically justified

separation of time scales which is not strictly dependent on the collisional mechanism assumed; therefore the method can be applied in all the cases when the dynamics on the magnetic surfaces is much faster than perpendicularly to them. A few general trends in the physics of a strongly rotating tokamak plasma, which appear, notwithstanding the relative simplicity of our model, to have been reported elsewhere [22].

## ACKNOWLEDGMENTS

The work reported in this paper is part of my doctoral dissertation. I wish to thank my advisors Professor K. Lackner and Professor D. J. Sigmar for their constant support and expert guidance, Professor C. Canuto and Dr. C. T. Hsu for several useful discussions. I did most of the work while at the Theory 3 Division, Max-Planck-Institute for Plasma Physics, Garching (FRG), as a EURATOM guest, and at the Plasma Fusion Center, Massachusetts Institute of Technology, Cambridge (USA), as a visiting scholar. The kind hospitality of these laboratories, which also provided computer time on the Cray machines at Garching and Livermore, is gratefully acknowledged. This paper is dedicated to I.G.

## REFERENCES

1. C. T. Hsu and D. J. Sigmar, MIT Report PFC/JA-88-14, 1988; *Plasma Phys. Controll. Fusion* (1990), in press.
2. R. Zanino, Ph.D. thesis, Politecnico di Torino, 1989 (unpublished). [Italian]
3. S. I. Braginskii, in *Reviews of Plasma Physics*, edited by M. A. Leontovich (Consultants Bureau, New York, 1965), Vol. 1.
4. P. H. Rutherford, *Phys. Fluids* **17**, 1782 (1974).
5. S. P. Hirshman and D. J. Sigmar, *Nucl. Fusion* **21**, 1079 (1981).
6. K. Brau *et al.*, *Nucl. Fusion* **23**, 1463 (1983); K. H. Burrell *et al.*, *Nucl. Fusion* **28**, 3 (1988); M. Mattioli *et al.*, *J. Appl. Phys.* **64**, 3345 (1988).
7. C. S. Chang and R. D. Hazeltine, *Nucl. Fusion* **20**, 1397 (1980).
8. K. H. Burrell, T. Ohkawa, and S. K. Wong, *Phys. Rev. Lett.* **47**, 511 (1981).
9. W. M. Stacey and D. J. Sigmar, *Phys. Fluids* **27**, 2076 (1984).
10. S. K. Wong, *Phys. Fluids* **30**, 818 (1987).
11. F. L. Hinton and R. D. Hazeltine, *Rev. Mod. Phys.* **48**, 239 (1976).
12. J. W. Connor *et al.*, *Plasma Phys. Controll. Fusion* **29**, 919 (1987).
13. D. J. Sigmar, R. Zanino, and C. T. Hsu, *Bull. Am. Phys. Soc.* **32-II**, 1917 (1987).
14. R. Zanino, MIT Report PFC/RR-88-4, 1988 (unpublished).
15. D. Gottlieb and S. A. Orszag, *Numerical Analysis of Spectral Methods* (SIAM, Philadelphia, 1977); C. Canuto *et al.*, *Spectral Methods in Fluid Dynamics* (Springer-Verlag, New York, 1988).
16. *NAG FORTRAN Library Manual*, Mark 11 (NAG, Oxford, 1984).
17. C. W. Gear, *Numerical Initial Value Problems in Ordinary Differential Equations* (Prentice-Hall, Englewood Cliffs, NJ, 1971).
18. H. S. Carslaw and J. C. Jaeger, *Conduction of Heat in Solids* (Clarendon Press, Oxford, 1959), p. 120.
19. M. N. Rosenbluth *et al.*, in *Proceedings, IV th International Conference on Plasma Physics and Controlled Nuclear Fusion Research* (IAEA, Vienna, 1971), Vol. 1, p. 495.
20. C. T. Hsu, D. J. Sigmar, and R. Zanino, Sherwood Controlled Fusion Theory Meeting 1988, Paper 3D9 (unpublished).
21. C. T. Hsu and D. J. Sigmar, ASDEX Seminar, Schloss Ringberg (FRG), September 1989 (unpublished).
22. R. Zanino, Max-Planck-Institut Report IPP 5/32; Plasma Theory Seminar, Schloss Ringberg (FRG), July 1989 (unpublished).
23. R. Zanino, K. Lackner, C. T. Hsu, and D. J. Sigmar, *Europhisics Conference Abstracts* **13B**, Part I, 443 (1989).